

# A Systematic Review of Fundus Image Analysis for Diagnosing Diabetic Retinopathy

Sumathi K.<sup>1</sup>, Sendhil Kumar K. S.<sup>2\*</sup>

Submitted: 06/12/2023 Revised: 16/01/2024 Accepted: 30/01/2024

**Abstract:** Retinal image analysis reflects the rapid expansion of medical infrastructure, and efficient artificial intelligence models are created. Diabetic Retinopathy (DR), a disorder of the eyes caused by diabetes, is the most prevalent cause of vision loss in the eyes. To maintain vision, early diagnosis is essential. The manual diagnosing process used by ophthalmologists is difficult and time-consuming. Machine learning and Deep learning models based on artificial intelligence are crucial in raising the system's accuracy. This survey discusses several recent approaches to image-preprocessing techniques, dataset descriptions, evaluation metrics, the backbone model for classification, and segmentation. Lesions such as hemorrhages, exudates, and microaneurysms in the Fundus images are identified using AI-based techniques for early DR diagnosis which prevent irreversible vision loss. To further categorize the severity of the disease, this survey includes pre-trained models for DR classification such as Alexnet, VGG, ResNet, DenseNet, and other models in addition to traditional CNN networks. Finally, challenges in the future scope are also addressed, which gives attention to the researcher for their future research.

**Keywords:** Classification, Deep Learning, Diabetic Retinopathy, Fundus Images, Segmentation

## 1. Introduction

A few of the imaging modalities that have been developed over time to evaluate the human eye include Optical Coherence Tomography (OCT), OCT Angiography (OCTA), Fundus Photography (FP), and Fluorescence Angiography (FA)[1]. However, "Fundus Imaging" has become increasingly popular due to its non-invasiveness and affordability. It uses a monocular camera, to capture the back of the eye onto a two-dimensional plane. A 2D fundus image can be used to identify biomarkers. Numerous of these biomarkers are crucial in the diagnosis of retinal disorders. By 2040, one in three individuals will suffer from DR, a condition that affects 700 million people globally. It is characterized by the presence of damaged blood vessels at the rear of the retina [2].

Microaneurysms are an early clinical symptom of DR appearing as small red spots on the retina. Hemorrhages are anatomical deformities that cause uneven forms in the inner layer of blood vessels and increase the chance of blood leaking from the vessels. These thin blood vessels may rupture and give rise to hemorrhages. Cotton-wool patches are another name for soft exudates. These are frequently round or oval, pale yellow, and caused by capillary occlusions that permanently impair the retina's ability to function. The leakage of plasma results in hard exudates, that are noticeable as yellow patches on the retina. They

have a sharp edge and span the outer layer.

In a typical fundus image, an Optical Disc (OD) forms the circular structure that is the brightest and appears yellow. It's critical to look for unusual OD forms, shapes, or sizes in the area to monitor for early changes that could result in vision loss. The central retinal artery, vein, and branches constitute Retinal Blood Vessels (RBVs). RBVs' branching pattern and segmentation can reveal information regarding a variety of medical conditions. Examining the retinal biomarkers described above can provide important insights into a few of the most common retinal illnesses and help with the diagnosis of these kinds of abnormalities.

Some of the key eye conditions that can cause blindness if not treated early are cataracts, glaucoma, Diabetic Retinopathy (DR), Diabetic Macular Edema (DME), and Age-Related Macular Degeneration (AMD). Manually diagnosing the disease using traditional methods takes time and is error-prone. The automatic identification of retinal illnesses is now feasible and cost-effective because of Artificial Intelligence (AI), Machine Learning (ML), and Deep Learning (DL) techniques-based medical screening systems.

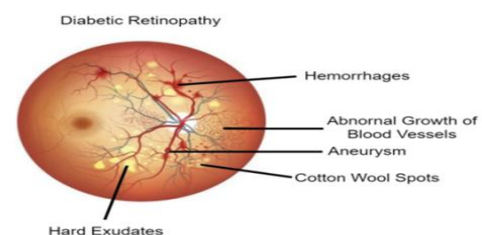


Fig 1. Lesions in Diabetic Retinopathy

<sup>1</sup>School of Computer Science and Engineering, Vellore Institute of Technology, Vellore, Tamil Nadu, orcid: 0009-0005-5766-9180

<sup>2\*</sup> Associate professor Senior, School of Computer Science and Engineering, Vellore Institute of Technology, Vellore, Tamil Nadu, orcid: 0000-0001-6669-9334

The proposed review's main objective is to examine various DL models that have recently been used to diagnose [3]–[6]utilizing fundus images. The review paper is structured as follows: The datasets utilized to study DR disease in the retina are shown in Section 2. In tabular form, section 3 presents evaluation metrics. Techniques for pre-processing images are outlined in section 4. The research studies that were examined related to backbone models for classification, segmentation of retinal blood vessels, and lesion detection are shown in Section 5. Section 6 presents a review of the literature along with the performance of recent research work on the diagnosis of DR disease related to relevant tasks. Following this, section 7, contains a list of potential future possibilities for this field of study. Finally, section 8 offers a conclusion.

## 2. Dataset for Retinal DR Disease Diagnosis

The size of the images in each dataset, the task, and the ground truth labels are all listed in the table below.

The Kaggle APTOS 2019 dataset includes 3662 fundus images from rural India from the Asia Pacific Tele-Ophthalmology Society's 2019 blindness detection dataset.: The training dataset is organized into five groups according to the International Clinical Diabetic Retinopathy Disease Severity Scale (ICDRSS). The following are the number of images: Healthy eye (1796), light NPDR (369), medium NPDR (995), extreme NPDR (193), and PDR (295) The 143 images in the Automated Retinal Image Analysis (ARIA)dataset were taken from adult male and females in the United Kingdom between 2004 and 2006. There are three markers to identify cases of DR, ARMD, and eyes in good condition. The Child's Heart Health Study in England (CHASE), a heart health study conducted in 299 primary schools in London between 2007 and 3008, created the CHASE-DB dataset. CHASE DB1 has 28 photos of 14 kids, two of which are from the child's cardiac and health and are 999x960 in size. On this dataset, retinal vascular segmentation is performed.

**TABLE 1.** Datasets of Fundus Images for DR Diagnosis

<i>The Dataset</i>	<i>Total Images</i>	<i>Image Dimensions</i>	<i>Task</i>	<i>True Ground Labels</i>
Kaggle APTOS 2019[7]	3662	Different size	DR Classification	1796 for normal eyes,369 for mild NPDR, 995 for Moderate NPDR,193 for severe NPDR (193), and PDR (295).
ARIA [8]	143	768x576	Normal eye, DR,	Healthy eye, age-related macular degeneration (ARMD), and DR cases
CHASE DB1[9]	28	999x960	Retinal vessel Segmentation	Blood Vessel Demarcation
DIRETDB0[10]	130	1500x1152	DR grading	110 symptoms DR, including neovascularization, SEs, and HEs
DIRETDB1[11]	89	1500x1152	DR grading	20 normal images
IDRiD[12]	516	4288x2848	Disease severity of DR, DEM detection	Grades of severity 81-MA, SE, EX, HE, OD,516-DR, and DME
DDR [13]	13673	Different size	DR grading	Annotation for the bounding box 13673-DRgrades 5 classes 757-MA, HE, SE, EX
DRIVE [14]	40	768x584	Retinal vessel Segmentation	33-Normal,7-Mild DR
E-Ophtha EX [15]	82	2544x1696 1440x960 2048x130	EX detection	47-Exudates,35 Normal Images
E-Ophtha MA [16]	381	2544x169 1440x960	MA detection	148-MAs,233 Normal images

Kaggle EyePACS [17]	88699	3000x2000	DR Grading	5-Stage DR grading
HRF [18]	45	3504x2336	Retinal Vessel Segmentation	15-Normal images,15-DRimages,15-Glaucoma Images
MESSIDOR [19]	1200	Different size	Diagnosis of DR, Optic Disc Segmentation	-
STARE [20]	400	700x605	Retinal vessel Segmentation	Annotated blood vessel segmentation on 20 images, pathology annotation on 10 images, and artery/vein labels on 10 images.

IDRiD (Indian Diabetic Retinopathy Image dataset) contains 516 images of size 4288x2848 annotated at a pixel level. DR lesions and detection of DME (Diabetic Macular Edema) are performed on this dataset. Contains image coordinates, but not segmentation masks, such as OD center, and the FOVEA. The Diabetic Retinopathy Database (DDR) contains 13673 fundus images obtained using a 45-degree field of view. This collection consists of 1151 ungradable images, 6266 normal images, and 6256 DR images. A bounding box for HM, MA, hard EX, and soft EX imaging modalities is added to 757 images to identify all DR lesions. The DRiDB dataset is made up of 50 images with annotations that describe the optic disc's blood vessel anatomy, neovascularization, and disease grade.

400 diabetic individuals between the ages of 25 and 90 made up the DRIVE (Digital Retinal Images for Vessel Extraction) dataset, which was gathered from a diabetic retinopathy screening program in the Netherlands. Retinal vessel segmentation is done on this 40-image dataset. The E-ophtha dataset contains two datasets. The first one is e-ophtha-MA which includes 148 images, MAs, and 233 healthy images, the other one is e-ophtha-EX which includes 47 images exudates, and 35 normal images.

In 2015, the State of California Healthcare Foundation sponsored the Kaggle EyePACS dataset. High-resolution images provided by EyePACS free platform for DR screening. There are 88699 images in it, 35126 of which are used for training. The class label is given on a scale of 0-4. Class labels for the healthy eye (25810), 1 for light DR (2443), 2 for medium DR (5292), 3 for serious DR (873), and 4 for PDR (708). DR grades are given by a single specialist according to the ICDRSS scale. A single specialist assigns DR grades using the ICDRSS scale. The HRF dataset contains 45 images, mainly used for blood vessel segmentation. 1200 color video camera-captured ocular fundus images are included in the Messidor dataset. At the University of California, STARE (structured Analysis of the retina) was launched.

### 3. Evaluation Metrics for DR

The DL model is assessed using several evaluation indicators during a DR diagnosis. The most popular evaluation measures are included in the following table along with their descriptions.

**TABLE 2.** Metrics for Performance Evaluation

Metric	Formula	Description
Accuracy	$Accuracy = \frac{TP + TN}{TP + TN + FP + FN}$	Calculate the percentage of patients the model properly classifies.
The AUC - ROC	Sensitivity - verse(1-Specificity) plot	Shows the area under the curve of receiver operating characteristic (AUC). AUC values above a certain threshold signify improved system performance
DSC coefficients (Dice)	$Dice = \frac{2TP}{2TP + FN + FP}$	Calculate how close the segmentation masks from the ground truth and the prediction are to each other.
Index of IoU/Jaccard	$IoU = \frac{TP}{FP + FN + TP}$	Calculate the segmentation mask overlap between the ground truth and forecast segments.
F1-Score	$F1 = \frac{2TP}{2TP + FN + FP}$	Determine the model's overall effectiveness in recognizing both positive as well as negative cases.
Precision (PRE)	$PRE = \frac{TP}{TP + FP}$	The precision shows what percentage of the positive results were true. Better performance is indicated by a higher PRE value.
Sensitivity/Recall	$SEN = \frac{TP}{TP + FN}$	The proportion of true positives that have been

call/TP R		classified to those that are present in the actual truth.
Specificity/FP R(SPE)	$SPE = TN / (TN + FP)$	The proportion of the actual negative in the base truth is categorized as the real true negative.  FPR (false positive rate) = $(1 - SPE)$

In this survey, most of the metrics are used to evaluate the proposed model with the already existing model used in other studies. The selection of the metrics to be utilized affects the assessment and contrast of different models. Using performance metrics like area under the Receiver Operating Characteristic Curve (AUC-ROC), and accuracy, the performance of the classification task is evaluated. In the segmentation task, metrics including the Jaccard index, the sensitivity, and the Dice Similarity Coefficient (DSC) are used.

#### 4. Image Pre-Processing

Image processing is required to ensure image consistency, improve image features, and eliminate noise from images.

Many pre-processing methods that are frequently applied to eye disorders are included in this section.

##### 4.1 Contrast Enhancement

The process of histogram equalization can be used to improve contrast in fundus images, Zhao et al [18], [21], which boosts the image's overall contrast while ignoring the local differences between them. Adaptive histogram equalization is a more sophisticated contrast enhancement technique that accounts for local differences surrounding a particular pixel. Contrast Limited Adaptive Histogram Equalization (CLAHE), addresses the problem of excessively enhanced contrast in the image's near-contrast region. By adjusting the image's contrast using appropriate preprocessing techniques, see the retina's intricate structure and more easily identify any abnormalities.

##### 4.2 Denoising and Normalisation

To eliminate noise from retinal images, non-local means denoising techniques, a median filter [22], and a Gaussian filter are some examples of noise removal techniques. More noise will be removed by a denoising algorithm, but the finer details in the images will be lost.

**TABLE 3.** Pre-processing techniques for the diagnosis of DR

<i>Study</i>	<i>Preprocessing Techniques</i>	<i>Methodology</i>	<i>Datasets</i>	<i>Evaluation (%)</i>
Ishtiaq et al [22]2023	Median filter, data augmentation, image resizing	GraphNet124, ResNet50, SVM	Kaggle EyePACS	ACC 98.85
Bilal et al [23]2022	Data Augmentation, Rotation, Shearing, Image flipping, Zoom, Cropping, Image translation	CNN SVD, Inception-V3	EyePACS-1, Messidor, DIARETDB0	ACC {97.92,94.59,93.52}
Abbood et al [24]2022	Circle Crop and Gaussian Blur	SVM, Logistic Regression, Decision tree	Kaggle, Messidor	ACC {92.0,93.6}
Jabbar et al [25] 2022	Non-local Mean Denoising (NLMD) Weighted Gaussian blur	VGGNet model	Kaggle EyePACS	ACC 96.6
Nneji et al [26] 2022	CLAHE, Contrast enhancement, and Canny edge detection (CECED)	Weighted fusion deep learning network (WFDLN), VGG-16and Inception V3	Kaggle, Messidor	ACC {98.5,98.0}

Chaudhary et al [21]2021	Contrast limited adaptive histogram equalization (CLAHE)	Order-zero and order-one 2DFourier-Bessel series expansion-based flexible analytic wavelet transform(2D-FBSE-WT), LDA, PCA	IDRiD, Messidor	Average accuracy for {DR 0.955, for DME 0.965}  {0.975 for DR,0.985 for DME}
Jinfeng et al [27] 2020	Resize, Normalization, augmentation	Two-deep CNN with an ensemble technique	Kaggle	Model1 ACC 80.36, Model2 ACC 78.13

The datasets were initially of different sizes. To get the images to the typical dimension, the dataset was resized. Next, the augmentation technique was applied to balance the data. Finally, a median filtering method was applied to eliminate noise from the images. Then, an unsharp masking filter was applied to improve the contrast of the image. Using the information from the Kaggle eyePAC dataset al [22] were able to classify the DR stages with 98.85% accuracy.

Bilal et al [23] used a variety of preprocessing methods, including top-bottom hat modification to enhance image quality (Green Channel Extraction) to extract more retinal detail than other methods, and image scaling to make all the images the same size. To prevent misclassification and overfitting, the data was augmented. The proposed model's accuracy in the EyePACS-1, Messidor, and DIARETDB0 datasets was 97.59%,93.52%and 97.92% respectively.

A method for improving the contrast and quality of images using both grayscale and RGB images was proposed by Abbood et al [24]. It incorporates two functionalities such as cropping images to eliminate unnecessary content from the grayscale images, and circle cropping and Gaussian blurring to remove noise. The CNN model achieved 92% and 93.6% accuracy when examined on two benchmark datasets namely the Messidor and Kaggle EyePACS.

Jabbar et al [25] introduced several preprocessing methods, including data augmentation and scaling, The EyePACS dataset contains images captured from different environmental settings, and techniques are applied to standardize the images. Using interpolation resizes the fundus images into uniform size. The thresholding operation is performed by setting the pixel value to zero to remove the black background. After that, more retinal data is extracted from the green channel than from the red or blue channels. Retinal images are enhanced using contrast-limited adaptive histogram equalization (CLAHE). To address this issue, misclassification results from an imbalanced dataset. The following data augmentation processes are carried out Gaussian-Space Theory (GST), Shearing, and zooming.

96.6% accuracy is obtained when the VGGNet model is tested on EyePACS.

The Contrast-Enhanced Canny Edge Detection (CECED)and the CLAHE images are two channels of fundus images that Nneji et al [26] offered. These images are used as preprocessing approaches. Fundus images with CECED give essential features, but images with CLAHE offer fewer histogram amplifications and more intensity. The weighted features from CLAHE and CECED are combined by the Weighted Fusion Deep Learning Network (WEDLN) to solve low-quality fundus image problems. On Messidor and Kaggle datasets, the WEDLN model yielded accuracy values of 98.5% and 98.0% respectively. According to Chaudhary et al[21], to categorize various degrees of DR and DME, the CLAHE per processing approach is applied to the IDRiD and Messidor datasets.

Jinfeng et al [27] applied preprocessing techniques such as resizing to maintain the original aspect ratio, and cropped patches to reduce training overhead, to avoid feature bias each image is mean normalized. Two deep ensemble CNN models yielded an accuracy of 80.36% and 78.13% respectively on the Kaggle dataset.

## 5. Deep Learning Concepts in DR Diagnosis

A branch of artificial intelligence called Deep Learning (DL) can extract characteristics from data without the need for hand-crafted.

features seen in machine learning models, and it can execute models with fewer demands on human resources. DL's ability to automatically learn features from complicated visual input data makes it appropriate for the analysis of medical images. We covered backbone models for analyzing image tasks in the section that follows.

### 5.1 Backbone Models for Classification Task

CNN, commonly referred to as ConvNets, is mostly used for object detection and image processing. It has numerous layers. The convolutional layer, Rectified Linear Unit

(ReLU), pooling layer, and fully connected layer constitute the CNN architecture. Several filters are applied by the convolutional layer to carry out the convolutional process. Apply a function to elements using the ReLU layer. This layer produces a rectified mapping of features as its output. The feature map is then adjusted and provided into the pooling layer, which reduces the feature map's dimensions. The pooling layer flattens the generated two-dimensional array to become a single continuous linear vector. The pooling layer's flattened matrix is offered as an input to build a fully connected layer, which classifies and recognizes images.

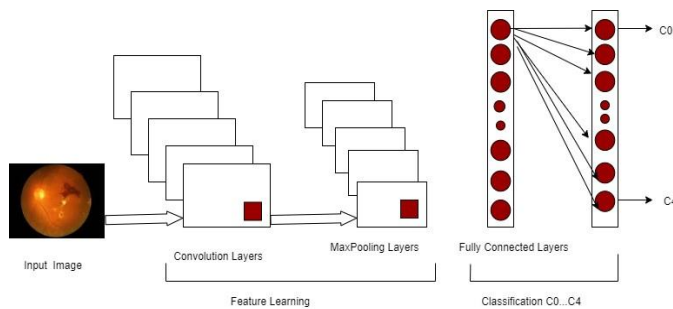


**Fig 2.** The basic Structure of a Convolutional Neural Network

Alexnet, a pre-trained convolutional neural network with eight layers deep, five layers of convolution, and three layers that are fully connected, was employed by Chandrasekaran et al [3]. The Rectified Linear Unit (ReLU) is the activation that is utilized. As AlexNet does exponentially well in natural image classification, it can classify medical images.

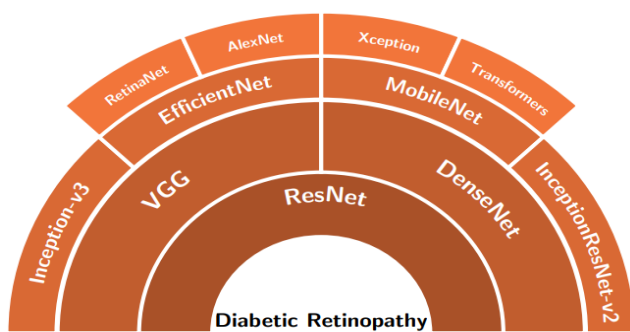


**Fig 3.** The various models for DR classification

The most widely utilized network structure for lesion categorization now is the Visual Geometry Group (VGG16, VGG19) variations of VGGNet, which were employed by Mohanty et al [18]. In addition to a fully connected layer, VGGNet has many convolutional blocks. In contrast to AlexNet, VGGNet uses 3x3 convolutions (pad 1) in place of AlexNet's 7x7 convolutions. To lower the resolution, a max pooling layer connects the convolution block, which consists of N 3x3 convolutions. Each class's projected probability comes from the fully connected layer. It is

suggested to use a Residual Neural Network (ResNet) to address the vanishing gradient issue caused by the deep neural network structure in VGG. There are multiple versions of ResNet, the most used ones are ResNet50 and ResNet101. ResNet's convolutional block provides identity mapping through a skip connection to VGG. The layer output is then added to the merged block.

DenseNet was utilized by Raja Sarobin M et al [28] to densely connected convolution networks, extending the residual process to all layers of convolution. Within the dense block, every layer transmits its unique feature maps to every layer that follows it and receives additional inputs from all subsequent layers. GoogleNet considered that numerous 1x1 convolutions should be used in place of other convolutions to lower the model's parametric number.

## 5.2 Backbone Models for Segmentation Task

**5.2.1 Fully Convolution Networks (FCNs)** perform convolution operations such as down-sampling and up-sampling. Each pixel in the down-sampled image shows the intensity that corresponds to the object's existence, providing more detailed information about the image being used in the form of miniature heat maps of various items. These mini-samples are combined with the highest probability class assigned to each pixel during the up-sampling to create a high-resolution segmentation map.

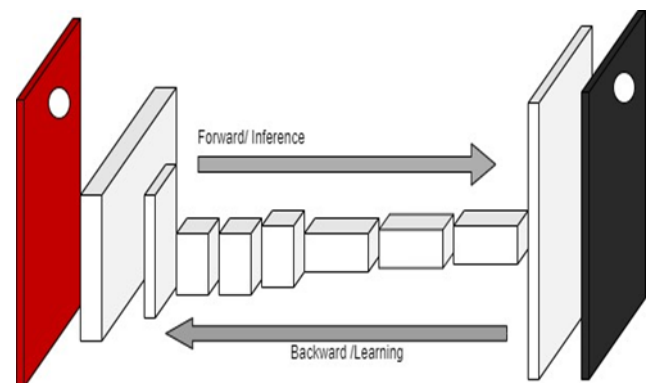


**Fig 4.** An FCN's (Fully Convolutional Network) basic architecture

Segmenting the lesions inside the image at the pixel level is the segmentation task. Blood vessel segmentation from retinal images is an important and difficult task in medical assessment and diagnosis. Retinal blood vessel segmentation is classified into different categories such as Vessel tracing/ tracking mathematical morphology, matched filter, model-based approach classified into vessel profile models and deformable models and multi-scale approaches, Rician Denoising algorithm and thresholding, and supervised classification algorithms.

## 5.2.2 Model U-Net

The U-Net network structure is a deep-learning architecture that supports the study of medical image segmentation. The

contracting path for down-sampling to gain context information and the Symmetric Expanding path for up-sampling to obtain precise position, constitute the two components of the U-Net network. U-Net network David et al [29] topology is frequently utilized and efficient for segmenting medical images.

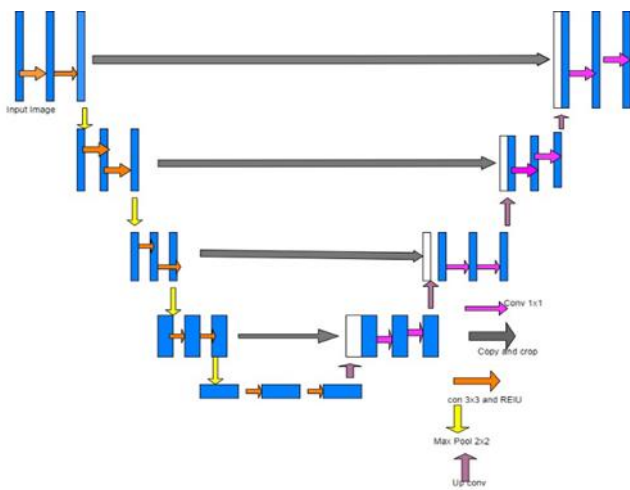


Fig 5. U-Net Architecture

### 5.3 Deep Learning Models for DR Detection Task

The detection task in the medical images defines the location of each object instance with a bounding box and is classified into single-stage and multi-stage models.

#### 5.3.1 Single-Stage Detection Models

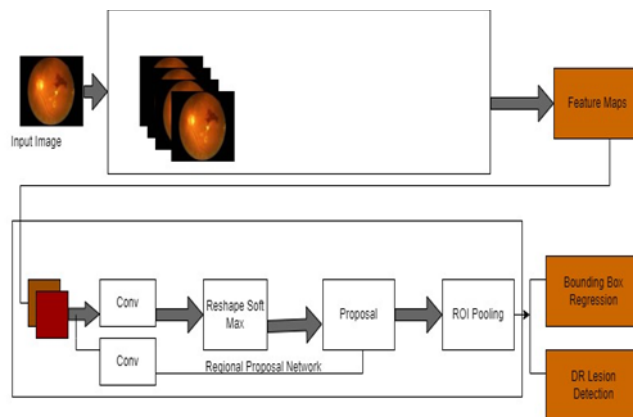


Fig 6. YOLOV3 pipeline for DR lesion detection

Most of the study focused on single-stage detection due to its timely performance and algorithm running rate, which removes region of interest extraction and directly classifies the candidate bounding box. The YOLO family of object detection models is called YOU ONLY LOOK ONCE(YOLO). YOLOV2 adds more anchor frames and fine-grained features, while YOLOV3 optimizes the network structure. YOLOV4 by [30] contains the optimization techniques.

#### 5.3.2 Models of Two-Stage Detection

The task is split into two parts by two-stage detection models. First, the region of interest is extracted, and then the extracted region is classified and regressed.

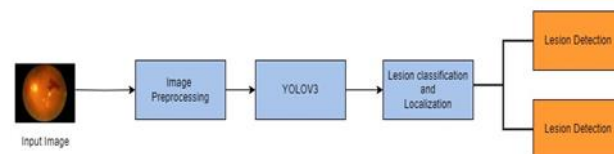


Fig 7. Two-Stage RFCNN Detection Models for DR

R-CNN families such as R-CNN Manan et al [31], Fast R-CNN which involves extraction of RoIs from the feature maps, Faster RCNN introduced region proposal network for generation RoIs by regressing and anchor boxes, and R-FCN uses the position-sensitive score maps, which involves two-stage object detection tasks.

TABLE 4. DR Diagnosis Methods

Study	Classifier	Feature Extraction Methods	Methodology	Datasets	Evaluation (%)
Mohanty et al [32]2023	XGBoost	VGG16	Two models of DL 1. A hybrid model that combines the XGBoost Classifier with the VGG16 2.DenseNet121 model	APTOS	ACC {79.50,97.30}

			Preprocessing techniques (resize, Gaussian Blur, BenGraham approach,		
Alwakid et al [33]2023	SoftMax	Inception-V3	A transfer DL(Inception-V3) 1. With image enhancement using CLAHE, ESRGAN (super-resolution generative adversarial network) 2. Without image enhancement	APTOS	The accuracy of enhancement is 98, without enhancement 80.87
Lin et al [34]2023	SoftMax	Revised ResNet-50	A preprocessing standard operating procedure (SOP) A redesigned ResNet-50 architecture A revised structure of ResNet-50(an adaptive learning score to modify the layer weights and visualization tools to extract relevant features)	Kaggle	Training accuracy is 0.8395, testing accuracy is 0,7432
Farag et al [35]2022	SoftMax	DenseNet169	DenseNet169 with the Convolutional Block Attention Module (CBAMK), circular crop, Principal Component Analysis (PCA),	APTOS	ACC, SEN, SPE, QWK (97, 97, 98.3, 0.9455)
AbdelMaksoud et al [36]2022	SoftMax	E-DenseNet	HEBPDS, GANs-based augmentation (Cropping, Rotation, Flipping), EyeNet, DenseNet,	EyePACS, APPTOS, MESSIDOR, IDRiD	ACC {96.8,84,91.6,93}, SEN{98.3,94,95,96.7} SPE {72,74,58,72}, DSC {98.3,87,95.1,96}

			DenseNet-BC, Adam Optimizer		QKS {0.97,0.8,0.91,0.94}
Raja Sarobin M et al [28]2022	SoftMax	DenseNet	CNN CNN with ResNet CNN with DenseNet, Augmentation, Image resizing, Transfer learning	Kaggle	ACC {75.61,93.18,96.22}
Chandrasekaran, et al[39]2022	SoftMax	AlexNet	Three CNN models with multi-resolution inputs (Custom CNN with a Hyper Analytic Wavelet (HW), a ResNet with attention along with HW activation, AlexNet for DR with HW activation)	Kaggle	AlexNet for DR has an accuracy of 98 a sensitivity of 99
Jabbar et al [25]2022	Multiclass	VGGNet	Resizing of interpolation images, weighted Gaussian blur, CLAHE	EyePACS	ACC 96.6
Kaushiket al [40] 2021	A single Meta-learner classifier		The stacked ensemble CNN model, mean square error (MSE), and the peak the ratio of signal to noise (PSNR) are used to measure luminosity normalization.	EyePACS	For binary class:  ACC 97.2, SEN 97.7, SPE 100  For multi-class: ACC 87.45,  SEN 96.30, SPE 97.25

## 6. Deep Learning in DR Diagnosis

### 6.1 DR Diagnosis

The accuracy of the hybrid model was 79.56%, and the accuracy of DenseNet121 was 97.30%, using the APTOS datasets for classification. Alwakid et al [33] Provided an Inception-V3 classification model for DR. The APTOS 2019 dataset was used to test this model. The accuracy of the first training example, which used CLAHE and ESRGAN to enhance the image, was 98.7%. The accuracy of the second training example, which did not use CLAHE

Mohanty et al. [32] To categorize fundus images into appropriate categories, a hybrid network that combines the VGG16 and XGBoost classifiers, and the two DenseNet121 network models has been proposed.

and ESRGAN, was 80.87%.

Lin et al. [34] updated the ResNet-50 model for DR grading developed. The fundus images utilized as input were pre-processed using a standard operating approach. An adjustable learning rate is incorporated into the revised ResNet-50 framework to alter the structure and adjust the layer weight. The proposed model was created to demonstrate the effects of visualizing the improved

ResNet50, not to provide an accurate DC. The model was tested using the Kaggle dataset, and the results indicated that the test accuracy was 0.7432 and the training accuracy was 0.8395. Farag et al [35]. The APTOS 2019 dataset was used to classify disease severity using the DenseNet169 model. From the fundus image, DenseNet was utilized to extract the features, and the convolutional block attention module subsequently refined the features. To address the class imbalance and predict severity, each feature was averaged using global average pooling and a weighted loss function.

The E-DenseNet model employed by Abdel Maksoud et al [36] can reliably identify standard and DR grades from images of the fundus. Both L1 as well as L2 regularization were applied to prevent overfitting. The accuracy, sensitivity, specificity, and dice similarity coefficients of this model, which were evaluated using four distinct benchmark datasets, were 91.6%, 95%, 95.1%, and 0.92, respectively. To categorize significant DR categories, Raja Sarobin M et al [28] developed two hybrid models CNN using ResNet and CNN using DenseNet. CNN using the ResNet model produced an accuracy of 93.18% on a data set of 3662 hybrid models; CNN using the Dense Net model did better by achieving an accuracy of 96.22%.

Chandrasekaran et al [37] used wavelet and spatial domain inputs in CNN models for DR classification. An ultra-analytical wavelet phase activation equation is developed for detailed parameter wavelet sub-bands. Hyper-activation function conditions were chosen to create effective and monotonic activations. The performance of three CNN models- custom CNN, ResNet using soft attention, and AlexNet using spatial-wavelet quilts was assessed. Among

these, AlexNet has the maximum sensitivity of 99% and the best accuracy level of 98% due to the modifications made to AlexNet for DR grading. Jabbar et al. [38] The main challenge of classifying medical images is the absence of labeled data. The issue is addressed by applying the transfer learning strategy, which reuses previously trained networks for identical problems. The author introduced a VGGNet model for DR classification was introduced by the author. The experiment's accuracy rate was 96.6% and it was run using the Kaggle EyePACS dataset.

## 6.2 Retinal Blood Vessel Segmentation

To prevent the loss, improve feature extraction, and lessen gradient disappearance, Wei et al [41] employed a multiscale attention network (MRANet that efficiently gathers vascular details using functional blocks like the multiple levels fusion of features block (MLF block), the focused attention block, and the MSR block. proposed UNet for the segmentation of blood vessels. AlexNet was introduced for image classification. The model is evaluated on the DRIVE, ARIA\_d, and MESSIDOR datasets. Liu et al [42] A Dual Attention Res2UNet model enhances blood vessel segmentation accuracy by replacing convolutional layers with Res2block and Drop block, obtaining multiscale information and reducing computation. Next, the explainable approach uses a trained fundus picture generator to explain the model. It shows that blood vessels can be distinguished when strip colors are varied in the fundus. The model training dataset is modified with noise addition, partial blurring, brightness adjustment, and enhancing precision.

**TABLE 5.** Blood Vessel Segmentation

<i>Study</i>	<i>Segmentation Methods</i>	<i>Methodology</i>	<i>Datasets</i>	<i>Evaluation (%)</i>
Wei et al [41]2023	Residual attention network on multiple scales	Blocks for multilevel feature fusion (MLF), attention, and multiscale residual connection (MSR)	DRIVE, CHASE_DB1	ACC {0.9698,0.9755} AUC Value {0.9899,0.9893}
Liu et al [42]2023	Dual Attention Res2UNet (DA-Res2UNet)	Dual attention, Spatial Attention	CHASE_DB1, DRIVE, STARE	F1 {81.88,82.77,83.96}
Wang et al [43]2023	Triple attention mechanism network with pre-activated convolution residual (PCRTAM-Net)	Technique for residual based on preactivated. dropout convolutions (Res-PDC) A residual down-sampled atrous convolutional spatial pyramid (Res-ACSP)	Drive, HRF, CHASE_DB1, and STARE	ACC {97.10,97.7,97.68,97.14} F1 {83.05,82.26, 84.64,81.16}

Gargari et al [44]2022	The model of U-Net++	CNN, Gaussian filter Gabor filter, Green Channel, Local binary pattern (LBP), Histogram of Oriented Gradients (HOG)	DRIVE, MESSIDOR	ACC, SE, SP, F1 {98.9,98.6}, {94.1,99}, {98.8,98} {98.14}
David et al [29]2022	UNet	Picture prospect map, patch probability map, Data augmentation, Adam law optimizer	DRIVE	SE, SP, ACC, Geometric mean {0.82, 0.98, 0.9661 0.8992}

Wang et al.[43] used the MS-CANet network consisting of an encoder, multiscale subtraction, and decoder. The encoder extracts semantic characteristics from 48 pixels of the original image, while the multiscale subtraction section improves vessel perception through multilevel and multi-stage subtraction procedures. The decoder retrieves feature maps gradually. Gargari et al. [44] introduced segmenting of the blood vessels using U-Net++ and deep CNN for classification. The matrices obtained from the Gabor filter are given as input to the UNet++ network. UNet++ learns the shape and structure of blood vessels and retinal tissue for segmentation and LBP and HOC methods for feature extraction from binary images are given as input to CNN. Finally, use 1D CNN for the diagnosis of retinal disease.

David et al. [29] proposed U-Net for the segmentation of retinal blood vessels. Multi-scale inputs and dense blocks are included to give high-quality results in segmentation. Using preprocessing the color retinal images are converted into grayscale. The image patches around the pixels of the vessel are used to generate the patch probability map, which is combined to produce the picture prospect maps of the picture. At last binary segmentation achieves higher accuracy compared to the traditional UNet.

### 6.3 Lesion Detection

#### 6.3.1MA Detection

Raudonis et al [45] applied ensemble-learning-based methods to automatically detect Microaneurysms. To achieve better accuracy and more consistent results, the suggested ensemble incorporates three distinct segmentation models, including UNet, UNE++, and ResNet34-UNet. By using a threshold value, a prediction map is created from each ROI. Comparing this model to the

other models, it obtained a higher IoU of 0.91 and a Dice value of 0.95 on fundus images. Soares et al [46] suggested a novel multiscale method for identifying potential microaneurysms. Two-stage neighborhood analysis is performed for MA labeling. In the first stage, the candidate shape is analyzed because candidate reshaping leads to improved MA labeling. In the second stage labels the region as true MA or false one. This model is evaluated on three datasets, namely Ophtha MA, Latin, and ROC Training. The Messidor data set is used for DR detection performance and achieved 80% specificity 98.73% sensitivity and 98.18% for at least one or two MAs detection.

#### 6.3.2 Hemorrhage Detection

Maqsood et al. [47]used 3D-CNN to detect hemorrhages. Using transfer learning, Contrast Limited Adaptive Histogram Equalization (CLAHE) is applied as a preprocessing step to improve the details of the edges from the input image, VGG19. An Extreme Learning Machine (ELM) model is then employed to detect hemorrhages. This method is validated with six datasets HRF, DRIVE, STARE, MESSIDOR, and DIARETDB0 achieved 99.98%, 99.98%, 95.12%, 99.38%, 95.53%, and 97.46% accuracy respectively.

#### 6.3.3 Exudates Detection

Manan et al [16]For localizing hard exudates on retinal image patches, a quicker R-CNN object detector with an SVM classifier has been developed. The SVM classifier pre-scanned input image patches based on the presence of exudates; patches that were identified as positive conducted object detector testing. On the e-Ophtha-EX dataset, this approach was examined, and the average accuracy was 84.7%.

**TABLE 6.** DR Lesion Detection Methods

Study	Lesion Detection methods	Methodology	Datasets	Evaluation (%)
Raudonis et al [45]2023	Ensemble-based model	Residual U-Net, U-Net++, and U-Net	PerDiRe	IoU (0.91) and dice score (0.95)
Soares et al [46],[47]2023	Multi-scale Approach	Green channel extraction, Region of interest (ROI),	Messidor	AUC 0.874, SEN 0.936

Maqsood et al [47]2021	3D CNN	Green Channel Extraction, Contrast Enhancement, VGG19	HRF, DRIVE, STARE, MESSIDOR, DIARETDB0, and DIARETDB1)	ACC {99.98, 99.98, 95.12, 99.38, 95.53, and 97.46}
Manan et al [16]2022	R-CNN object detector	ResNet-50, SVM	E-ophtha-EX	FI score0.8367
Kurilová et al [48]2021	RTC-Net model	Data augmentation	E-Ophtha, HEI-MED, DIARETDB	ACC {99,98,98} SEN {92,95,97}
Alyoubi et al [30]2021	YOLOV3	NN512, Colour Normalizing, Data Augmentation	DDR	ACC 89, SEN 89, SPE 97.3

Kurilová et al [48]To find the exudates, semantic segmentation was used to examine pixel-based areas. The encoder that learns the properties of the pixel can utilize a semantic segmentation model. To determine a dense rating, the decoder must visualize the encoder's resolution characteristics. Fewer convolution layers are used by RTC-N350 to up-sample the image as greater convolution causes noise in the image. Network complexity is decreased by using the feature identity and non-identity mapping and unpooling layers. Alyoubi et al. [30]presented two deep-learning models to classify DR into five stages. To classify DR, CNN512 used the entire image as input. APTOS and Kaggle 2019 datasets were used to evaluate this model, and it received accuracy scores of 84.1% and 88.6% respectively. The other model was YOLOv3 to localize and detect DR lesions on the DDR dataset and obtained 89% accuracy and 97.3% specificity and 98% sensitivity. YOLOv3 was the alternative model that was used to locate and identify lesions associated with DR on the DDR dataset. It achieved 89% accuracy,97.3% specificity, and 98% sensitivity.

## 7. Challenges and Future Directions in DR Analysis

Referring to the fundus, OCT, and other modalities, ophthalmologists make decisions. Fundus images are utilized in the diagnosis of glaucoma and NPDR, whereas OCT is employed to diagnose age-related macular degeneration and Diabetic Macular Edema (DME). Most studies that are currently accessible only employed one modality.

Annotations are varied for diverse purposes in medical image analysis, like segmentation, prediction, and classification. The quantity of training data that is available for medical purposes is limited, and this has an impact on the model's performance. In this case, transfer learning techniques can be used, but they are constrained by the samples in the origin domain. Transferring knowledge from the domain of origin to the target domain can be accomplished through sample-based or feature-based

methods.

To avoid misclassification and eliminate manual feature extraction, unsupervised learning techniques carry out DR image classification tasks. Accurate disease diagnosis depends on a significant amount of data samples for learning due to the adaptive characteristics of learned models.

This makes it possible to continue developing deep-learning models for medical imaging in response to the challenges. During image segmentation, there are smaller differences between classes and more variability within classes. The network is enhanced with the incorporation of the attention mechanism, which places a small region between the target regions and the surrounding information.

Due to a shortage of sample data, supervised learning is used to improve unsupervised learning applications. The model's performance, which is essential for image analysis, can be improved by incorporating sample data into model training along with visual adversarial network architecture.

The detection and classification of ocular disorders focus on retinal maculopathy. The retina's macula is situated at its center. A few ocular conditions, including Diabetic Macular Edema (DME) and Age-Related Macular Degeneration (AMD), can affect eye health. The buildup of excess fluid behind the pigment of the retina cell indicates the early stages of AMD cells. Retinal pigment cells are damaged by choroidal warts. Abnormal and leaky vascular development is indicative of the end stage of AMD. These are progressive diseases that lead to blurred vision. Early diagnosis can prevent vision impairment.

Another type of eye-related disease is glaucoma which damages the optic nerves and causes vision loss resulting from increasing ocular pressure on the optic nerves. Early diagnosis of glaucoma is important to prevent losing sight.

## 8. Conclusion

An automated system is needed for the lack of ophthalmologists compared with the disease-affected

patients. The variety of eye-related lesions brings attention to researchers in terms of different kinds of imaging modalities in medical image analysis tasks. For automated DR diagnosis connected to the eyes, a variety of AI-based algorithms are put into practice and tested. Enhanced image pre-processing techniques are utilized to bring quality and significant features from the input images. Lesions such as hemorrhages, exudates, and microaneurysms that slightly differ from each other in terms of the number of pixels in the Fundus images are identified using AI-based techniques for early DR diagnosis which prevent irreversible vision loss.

This survey showed the latest AI-based approaches for eye-related DR diagnosis including DR classification, segmentation, and lesion detection. The proposed models reviewed in this survey depend on publicly available datasets. The images in the dataset were captured in different environmental conditions, not in a standard size to train the models. Thus, suitable preprocessing methods for images were used, including scaling, noise reduction, data augmentation, contrast improvement, and filtering. A balanced data set can help build a robust model that can be implemented in clinical use.

Several backbone models have been used in recent studies for both segmentation and classification tasks. The many types of lesions shown in fundus images were accurately classified by segmentation tasks using fully convolutional networks, U-Net, and its variants. For the classification task, the CNN network, AlexNet, the VGG, ResNet, and DenseNet were employed to precisely categorize DR severity stages and grad. Single-stage and multistage detection models used Regions of interest (RoIs) to locate different lesions in the input images. And then this survey presented a comparison of various existing studies based on the performance of models used in those existing studies for DR diagnosis. Finally, this study shows the challenges and the future scope for other retinal eye disease diagnoses.

## References

- [1] M. Elsharkawy et al., "The Role of Different Retinal Imaging Modalities in Predicting Progression of Diabetic Retinopathy: A Survey," *Sensors*, vol. 22, no. 9, p. 3490, May 2022, doi: 10.3390/s22093490.
- [2] P. Camargo-Plazas et al., "Diabetes self-management education for older adults in Western countries: a scoping review protocol," *JBI Evid Synth*, vol. 21, no. 5, pp. 993–1000, May 2023, doi: 10.11124/JBIES-22-00254.
- A. Sebastian, O. Elharrouss, S. Al-Maadeed, and N. Almaadeed, "A Survey on Diabetic Retinopathy Lesion Detection and Segmentation," *Applied Sciences*, vol. 13, no. 8, p. 5111, Apr. 2023, doi: 10.3390/app13085111.
- [3] M. S. Farooq et al., "Untangling Computer-Aided Diagnostic System for Screening Diabetic Retinopathy Based on Deep Learning Techniques," *Sensors*, vol. 22, no. 5, p. 1803, Feb. 2022, doi: 10.3390/s22051803.
- [4] M. W. Nadeem, H. G. Goh, M. Hussain, S.-Y. Liew, I. Andonovic, and M. A. Khan, "Deep Learning for Diabetic Retinopathy Analysis: A Review, Research Challenges, and Future Directions," *Sensors*, vol. 22, no. 18, p. 6780, Sep. 2022, doi: 10.3390/s22186780.
- [5] M. Elsharkawy et al., "The Role of Different Retinal Imaging Modalities in Predicting Progression of Diabetic Retinopathy: A Survey," *Sensors*, vol. 22, no. 9, p. 3490, May 2022, doi: 10.3390/s22093490.
- [6] M. Shaban et al., "A convolutional neural network for the screening and staging of diabetic retinopathy," *PLoS One*, vol. 15, no. 6, p. e0233514, Jun. 2020, doi: 10.1371/journal.pone.0233514.
- [7] S. G. Kobat et al., "Automated Diabetic Retinopathy Detection Using Horizontal and Vertical Patch Division-Based Pre-Trained DenseNET with Digital Fundus Images," *Diagnostics*, vol. 12, no. 8, p. 1975, Aug. 2022, doi: 10.3390/diagnostics12081975.
- [8] Z. CUI, S. SONG, and J. QI, "MF2ResU-Net: a multi-feature fusion deep learning architecture for retinal blood vessel segmentation," *Digital Chinese Medicine*, vol. 5, no. 4, pp. 406–418, Dec. 2022, doi: 10.1016/j.dcm.2022.12.008.
- [9] U. Bhimavarapu and G. Battineni, "Deep Learning for the Detection and Classification of Diabetic Retinopathy with an Improved Activation Function," *Healthcare*, vol. 11, no. 1, p. 97, Dec. 2022, doi: 10.3390/healthcare11010097.
- [10] L. Math and R. Fatima, "Adaptive machine learning classification for diabetic retinopathy," *Multimed Tools Appl*, vol. 80, no. 4, pp. 5173–5186, Feb. 2021, doi: 10.1007/s11042-020-09793-7.
- [11] T. Selçuk, A. Beyoğlu, and A. Alkan, "Automatic detection of exudates and hemorrhages in low - contrast color fundus images using multi semantic convolutional neural network," *Concurr Comput*, vol. 34, no. 6, Mar. 2022, doi: 10.1002/cpe.6768.
- [12] S. Patel, M. Lohakare, S. Prajapati, S. Singh, and N. Patel, "DiaRet: A Browser-Based Application for the Grading of Diabetic Retinopathy with Integrated Gradients," in *2021 IEEE International Conference on Robotics, Automation and Artificial Intelligence (RAAI)*, IEEE, Apr. 2021, pp. 19–23. doi: 10.1109/RAAI52226.2021.9507938.
- [13] T. Li, Y. Gao, K. Wang, S. Guo, H. Liu, and H. Kang, "Diagnostic assessment of deep learning algorithms for diabetic retinopathy screening," *Inf Sci (N Y)*, vol. 501, pp. 511–522, Oct. 2019, doi: 10.1016/j.ins.2019.06.011.
- [14] X. Deng and J. Ye, "A retinal blood vessel segmentation based on improved D-MNet and pulse-

- coupled neural network,” *Biomed Signal Process Control*, vol. 73, p. 103467, Mar. 2022, doi: 10.1016/j.bspc.2021.103467.
- [15] M. A. Manan, T. M. Khan, A. Saadat, M. Arsalan, and S. S. Naqvi, “A Residual Encoder-Decoder Network for Segmentation of Retinal Image-Based Exudates in Diabetic Retinopathy Screening,” Jan. 2022, [Online]. Available: <http://arxiv.org/abs/2201.05963>
- [16] Subhasree, J. B. Princess, and Salaja, “Analysis and Automatic Detection of Microaneurysms in Diabetic Retinopathy using transfer learning,” in *2022 6th International Conference on Computation System and Information Technology for Sustainable Solutions (CSITSS)*, IEEE, Dec. 2022, pp. 1–7. doi: 10.1109/CSITSS57437.2022.10026377.
- [17] M. K. Jabbar, J. Yan, H. Xu, Z. Ur Rehman, and A. Jabbar, “Transfer Learning-Based Model for Diabetic Retinopathy Diagnosis Using Retinal Images,” *Brain Sci*, vol. 12, no. 5, p. 535, Apr. 2022, doi: 10.3390/brainsci12050535.
- [18] Z. A. Elaouber, A. Feroui, M. E. A. Lazouni, and M. Messadi, “Blood vessel segmentation using deep learning architectures for aid diagnosis of diabetic retinopathy,” *Comput Methods Biomech Biomed Eng Imaging Vis*, vol. 11, no. 4, pp. 1463–1477, Jul. 2023, doi: 10.1080/21681163.2022.2145999.
- [19] Y. Prajna and M. K. Nath, “Efficient blood vessel segmentation from color fundus image using deep neural network,” *Journal of Intelligent & Fuzzy Systems*, vol. 42, no. 4, pp. 3477–3489, Mar. 2022, doi: 10.3233/JIFS-211479.
- [20] P. K. Chaudhary and R. B. Pachori, “Automatic Diagnosis of Different Grades of Diabetic Retinopathy and Diabetic Macular Edema Using 2-D-FBSE-FAWT,” *IEEE Trans Instrum Meas*, vol. 71, pp. 1–9, 2022, doi: 10.1109/TIM.2022.3140437.
- [21] U. Ishtiaq, E. R. M. F. Abdullah, and Z. Ishtiaque, “A Hybrid Technique for Diabetic Retinopathy Detection Based on Ensemble-Optimized CNN and Texture Features,” *Diagnostics*, vol. 13, no. 10, p. 1816, May 2023, doi: 10.3390/diagnostics13101816.
- [22] Bilal, L. Zhu, A. Deng, H. Lu, and N. Wu, “AI-Based Automatic Detection and Classification of Diabetic Retinopathy Using U-Net and Deep Learning,” *Symmetry (Basel)*, vol. 14, no. 7, p. 1427, Jul. 2022, doi: 10.3390/sym14071427.
- [23] S. H. Abbood, H. N. A. Hamed, M. S. M. Rahim, A. Rehman, T. Saba, and S. A. Bahaj, “Hybrid Retinal Image Enhancement Algorithm for Diabetic Retinopathy Diagnostic Using Deep Learning Model,” *IEEE Access*, vol. 10, pp. 73079–73086, 2022, doi: 10.1109/ACCESS.2022.3189374.
- [24] M. K. Jabbar, J. Yan, H. Xu, Z. Ur Rehman, and A. Jabbar, “Transfer Learning-Based Model for Diabetic Retinopathy Diagnosis Using Retinal Images,” *Brain Sci*, vol. 12, no. 5, p. 535, Apr. 2022, doi: 10.3390/brainsci12050535.
- [25] G. U. Nneji, J. Cai, J. Deng, H. N. Monday, M. A. Hossin, and S. Nahar, “Identification of Diabetic Retinopathy Using Weighted Fusion Deep Learning Based on Dual-Channel Fundus Scans,” *Diagnostics*, vol. 12, no. 2, p. 540, Feb. 2022, doi: 10.3390/diagnostics12020540.
- [26] G. Jinfeng, S. Qummar, Z. Junming, Y. Ruxian, and F. G. Khan, “Ensemble Framework of Deep CNNs for Diabetic Retinopathy Detection,” *Comput Intell Neurosci*, vol. 2020, pp. 1–11, Dec. 2020, doi: 10.1155/2020/8864698.
- [27] Y. R., V. Raja Sarobin M., R. Panjanathan, G. J. S., and J. A. L., “Diabetic Retinopathy Classification Using CNN and Hybrid Deep Convolutional Neural Networks,” *Symmetry (Basel)*, vol. 14, no. 9, p. 1932, Sep. 2022, doi: 10.3390/sym14091932.
- [28] S. A. David, C. Mahesh, V. D. Kumar, K. Polat, A. Alhudaif, and M. Nour, “Retinal Blood Vessels and Optic Disc Segmentation Using U-Net,” *Math Probl Eng*, vol. 2022, pp. 1–11, Feb. 2022, doi: 10.1155/2022/8030954.
- [29] W. L. Alyoubi, M. F. Abulkhair, and W. M. Shalash, “Diabetic Retinopathy Fundus Image Classification and Lesions Localization System Using Deep Learning,” *Sensors*, vol. 21, no. 11, p. 3704, May 2021, doi: 10.3390/s21113704.
- [30] T. M. K. A. S. M. A. S. S. N. Malik A. Manan, “A Residual Encoder-Decoder Network for Segmentation of Retinal Image-Based Exudates in Diabetic Retinopathy Screening”.
- [31] C. Mohanty et al., “Using Deep Learning Architectures for Detection and Classification of Diabetic Retinopathy,” *Sensors*, vol. 23, no. 12, p. 5726, Jun. 2023, doi: 10.3390/s23125726.
- [32] G. Alwakid, W. Gouda, and M. Humayun, “Deep Learning-Based Prediction of Diabetic Retinopathy Using CLAHE and ESRGAN for Enhancement,” *Healthcare*, vol. 11, no. 6, p. 863, Mar. 2023, doi: 10.3390/healthcare11060863.
- [33] C.-L. Lin and K.-C. Wu, “Development of revised ResNet-50 for diabetic retinopathy detection,” *BMC Bioinformatics*, vol. 24, no. 1, p. 157, Apr. 2023, doi: 10.1186/s12859-023-05293-1.
- [34] M. M. Farag, M. Fouad, and A. T. Abdel-Hamid, “Automatic Severity Classification of Diabetic Retinopathy Based on DenseNet and Convolutional Block Attention Module,” *IEEE Access*, vol. 10, pp. 38299–38308, 2022, doi: 10.1109/ACCESS.2022.3165193.
- [35] E. AbdelMaksoud, S. Barakat, and M. Elmogy, “A computer-aided diagnosis system for detecting various diabetic retinopathy grades based on a hybrid deep learning technique,” *Med Biol Eng Comput*, vol. 60,

- no. 7, pp. 2015–2038, Jul. 2022, doi: 10.1007/s11517-022-02564-6.
- [36] Sebastian, O. Elharrouss, S. Al-Maadeed, and N. Almaadeed, “A Survey on Deep-Learning-Based Diabetic Retinopathy Classification,” *Diagnostics*, vol. 13, no. 3, p. 345, Jan. 2023, doi: 10.3390/diagnostics13030345.
- [37] M. K. Jabbar, J. Yan, H. Xu, Z. Ur Rehman, and A. Jabbar, “Transfer Learning-Based Model for Diabetic Retinopathy Diagnosis Using Retinal Images,” *Brain Sci*, vol. 12, no. 5, p. 535, Apr. 2022, doi: 10.3390/brainsci12050535.
- [38] Sebastian, O. Elharrouss, S. Al-Maadeed, and N. Almaadeed, “A Survey on Diabetic Retinopathy Lesion Detection and Segmentation,” *Applied Sciences*, vol. 13, no. 8, p. 5111, Apr. 2023, doi: 10.3390/app13085111.
- [39] H. Kaushik, D. Singh, M. Kaur, H. Alshazly, A. Zaguia, and H. Hamam, “Diabetic Retinopathy Diagnosis From Fundus Images Using Stacked Generalization of Deep Models,” *IEEE Access*, vol. 9, pp. 108276–108292, 2021, doi: 10.1109/ACCESS.2021.3101142.
- [40] S. Yi, Y. Wei, G. Zhang, T. Wang, F. She, and X. Yang, “Segmentation of retinal vessels based on MRANet,” *Heliyon*, vol. 9, no. 1, p. e12361, Jan. 2023, doi: 10.1016/j.heliyon.2022.e12361.
- [41] R. Liu, T. Wang, X. Zhang, and X. Zhou, “DA-Res2UNet: Explainable blood vessel segmentation from fundus images,” *Alexandria Engineering Journal*, vol. 68, pp. 539–549, Apr. 2023, doi: 10.1016/j.aej.2023.01.049.
- [42] H.-D. Wang et al., “PCRTAM-Net: A Novel Pre-Activated Convolution Residual and Triple Attention Mechanism Network for Retinal Vessel Segmentation,” *J Comput Sci Technol*, vol. 38, no. 3, pp. 567–581, Jun. 2023, doi: 10.1007/s11390-023-3066-4.
- [43] M. S. Gargari, M. H. Seyedi, and M. Alilou, “Segmentation of Retinal Blood Vessels Using U-Net++ Architecture and Disease Prediction,” *Electronics (Basel)*, vol. 11, no. 21, p. 3516, Oct. 2022, doi: 10.3390/electronics11213516.
- [44] V. Raudonis et al., “Automatic Detection of Microaneurysms in Fundus Images Using an Ensemble-Based Segmentation Method,” *Sensors*, vol. 23, no. 7, p. 3431, Mar. 2023, doi: 10.3390/s23073431.
- [45] Soares, M. Castelo-Branco, and A. Pinheiro, “Microaneurysms detection in retinal images using a multi-scale approach,” *Biomed Signal Process Control*, vol. 79, p. 104184, Jan. 2023, doi: 10.1016/j.bspc.2022.104184.
- [46] S. Maqsood, R. Damaševičius, and R. Maskeliūnas, “Hemorrhage Detection Based on 3D CNN Deep Learning Framework and Feature Fusion for Evaluating Retinal Abnormality in Diabetic Patients,” *Sensors*, vol. 21, no. 11, p. 3865, Jun. 2021, doi: 10.3390/s21113865.
- [47] V. Kurilová, J. Goga, M. Oravec, J. Pavlovičová, and S. Kajan, “Support vector machine and deep-learning object detection for localisation of hard exudates,” *Sci Rep*, vol. 11, no. 1, p. 16045, Aug. 2021, doi: 10.1038/s41598-021-95519-0.